Available online at www.sciencedirect.com

jmr&t Journal of Materials Research and Technology

journal homepage: www.elsevier.com/locate/jmrt

Original Article

Novel low modulus beta-type Ti–Nb alloys by gallium and copper minor additions for antibacterial implant applications

Ludovico Andrea Alberta[*], *Jithin Vishnu, Avinash Hariharan, Stefan Pilz, Annett Gebert, Mariana Calin*

Institute for Complex Materials, Leibniz Institute for Solid State and Materials Research Dresden (IFW Dresden), Helmholtzstr. 20, D-01069 Dresden, Germany

ARTICLE INFO

Article history:
Received 17 May 2022
Accepted 20 August 2022
Available online 24 August 2022

Keywords:
Low modulus beta titanium alloy
Antibacterial gallium and copper
Orthopedic implant
Mechanical properties
Corrosion

ABSTRACT

This study aims to develop novel low-modulus, corrosion-resistant Ti-based alloys with enhanced antimicrobial properties for bone-related implant applications. Novel β-type (Ti–45Nb)-based alloys with minor additions of the antibacterial elements Ga and/or Cu (up to 4 wt.%) were produced by a two-step casting process followed by homogenization treatment. Three nominal compositions $(Ti–45Nb)_{96}$-4 Ga, $(Ti–45Nb)_{96}$–4Cu and $(Ti–45Nb)_{96}$-2 Ga–2Cu (wt.%) were prepared based on alloy design approach using $[Mo]_{eq}$ and electron per atom (e/a) ratio. The influence of Ga and/or Cu addition on the phase constitution, mechanical response and corrosion characteristics in simulated body fluids (PBS, 37.5 °C) has been investigated. X-ray diffraction studies displayed a single β phase structure for all alloys, with an observed lattice contraction evidenced by the reduction of lattice parameters during Rietveld analysis. Homogenous equiaxed microstructures with grain sizes ranging from 55 μm up to 323 μm were observed for $(Ti–45Nb)_{96}$-4 Ga, $(Ti–45Nb)_{96}$-2 Ga–2Cu and $(Ti–45Nb)_{96}$–4Cu alloys. The alloys displayed excellent plasticity with no cracking, or fracturing during compression tests. Their tensile strength, Young's modulus, maximum tensile strain and elastic energy were measured in the ranges of 544–681 MPa, 73–78 GPa, 17–28% and 2.5–3.7 MJ/m^3, in the order $(Ti–45Nb)_{96}$-4 Ga > $(Ti–45Nb)_{96}$-2 Ga–2Cu > $(Ti–45Nb)_{96}$–4Cu. In addition, it has been observed that micro-alloying Ti–Nb alloy with Ga and/or Cu posed no deleterious effect on the corrosion resistance in simulated body fluid conditions. The improvement in strength of the developed alloys has been discussed based on grain boundary and solid-solution strengthening, whereas the improved plasticity is attributed to work hardening.

* Corresponding author.
E-mail address: l.a.alberta@ifw-dresden.de (L.A. Alberta).

https://doi.org/10.1016/j.jmrt.2022.08.111

1. Introduction

Titanium and its alloys are considered to be the most attractive metallic materials for load-bearing biomedical applications [1]. Diverse applications of these alloys encompass components for bone replacement (spinal correction and fixation devices, tibial components, bone plates, screws, mesh, rods), dental (artificial roots, orthodontic wires) and surgical devices (dental drills, forceps, laser electrodes) [2]. Compared to other commercial metallic biomaterials (e.g. austenitic stainless steel and Co–Cr alloys), Ti alloys have superior biocompatibility combined with low density and elastic modulus much more similar to that of human bones [1]. Despite these advantages, the implants can sometimes fail under the combination of stress, bacteria contamination and corrosion. For the widely used biomedical Ti alloys such as Ti–6Al–4V and Ti–6Al–7Nb, long-term studies have indicated the development of health disorders elicited by the release of metallic ions including aluminum (e.g. neurodegenerative diseases such as Alzheimer's disease and Parkinson's disease [3]) and vanadium (e.g. genetic damage [4]). In addition, these alloys possess higher elastic moduli (E = 105–114 GPa), compared to cortical bone (E = 10–32 GPa). Clinical studies have shown that such stiffer implant materials will impede the load transfer to the surrounding bone tissues (stress shielding), rendering native bone weaker, resulting in bone resorption and eventual loosening of the prosthetic devices [5].

To overcome these problems, a new generation of biocompatible and low modulus metastable β-type Ti alloys has been developed. Among all β-stabilized Ti-alloy systems, the Ti–Nb system and its alloys have received immense attention owing to its excellent display of lower elastic modulus, good ductility, high corrosion resistance, superior biocompatibility, superelastic and shape memory behavior [6–8]. The biomechanical and biochemical properties of these alloys can be tuned by proper control of phase transformation during thermomechanical processing [9,10], by design of porous materials [11–14] or by selective alloying [15–17]. By rapid cooling from the high-temperature β-phase field to room temperature, metastable states composed of body-centered cubic (bcc) β-phase, martensitic phases (hexagonal α′ and orthorhombic α″), hexagonal/trigonal ω-phase or a combination of them can be obtained [9,10]. Among these, the ω-phase exhibits the highest E and E varies strongly with Nb composition for α″ and β: $E_{\omega} > E_{\alpha'} > E_{\alpha''} > E_{\beta}$ [18]. The stability of the β phase represents an important parameter when developing low modulus Ti-based alloys: it determines whether, and in which amount, the martensitic transformations take place in response to either a mechanical (e.g. deformation) or thermal (e.g. quenching) driving force. Deformation-induced martensitic transformations are a function of β phase stability [19]. Depending on the stability of the β-phase, on the extent and direction of deformation, several deformation mechanisms could be activated, among which stress-induced martensite (SIM), twinning and dislocation slip, the latter being the dominant one in heavily stabilized β-Ti alloys [15,20–23]. Among these, stress-induced phase transformation as well as mechanical twinning are dominant in β systems where β phase is unstable. Further lowering of the Young's modulus can be achieved by alloying. Recently, the low-modulus β-type (Ti–40Nb)-xIn alloy system (where x = 3.5, 5 wt.%) was investigated. The newly developed Ti–Nb–In alloys demonstrated lower values of E in the range of 49–58 GPa in the solution-treated and water-quenched state as well as after different thermomechanical processing steps (annealing, solution treatment, hot or cold rolling with various thickness reduction) [24,25].

Another major cause of implant failure is the biomaterial-associated infections by multidrug-resistant bacteria which contaminate and adhere onto the implant surface, forming biofilm [26]. Antibiotic treatments are often ineffective; hence there is a need for alternative solutions. For Ti-based biomaterials, alloying or doping with antibacterial elements can render resistance against bacterial adhesion and biofilm formation by either contact-killing or agent release [27]. Among the various possible antibacterial alloying options (such as Zn, Ag, etc.), gallium (Ga) and copper (Cu) represent pertinent candidates in terms of clinical potential. Alloying titanium with Ga and Cu can improve not only the antibacterial properties but also the mechanical behavior and casting capabilities (low melting point cast Ti-based alloys) [28,29].

Gallium, which is already in use as a diagnostic and therapeutic tool in the medical field, is recently gaining recognition as a prospective inorganic antimicrobial agent to treat bacterial infections. Antibacterial effect of Ga can be explained by the so-called "Trojan horse" strategy which uses the gallium to disrupt bacterial iron metabolism [30–33]. Apart from this antibacterial activity, Ga is able to stimulate bone formation, without significant toxicity and discretely act on osteoclasts and osteoblasts for an improved osseointegration [34,35]. The use of Ga in dentistry is well-known, as many Ti–Ga amalgams have been studied in terms of structure, mechanical properties, corrosion resistance, cytotoxicity and antibacterial capacity [36,37]. Recent studies on metallurgical Ga additions to Ti–Al–Zr–Si alloys demonstrated highly efficient antibacterial activity without any cytotoxic effect, even with minor Ga concentrations of 1–2 wt.% [38]. Addition of Ga to Ti–Nb based alloys has been investigated for superelasticity and shape-memory effects in Ti–24Nb–3Ga and Ti–18Nb–3Ga (at.%) [39,40]. However, little to no literature is available regarding Ga-bearing Ti–Nb-based alloys with retained β phases for low modulus load-bearing implant material applications.

On the other side, Cu is a natural trace element found in the human body, essential for the proper functioning of organs and metabolic processes [41]. Cu was proved to exhibit antibacterial effects on a wide spectrum of bacterial species [42–45]. The antibacterial properties of Cu-containing titanium alloys are strongly dependent on the Cu content and Cu form (in solid solution or intermetallic compound) [46–48]. Many Cu-bearing Ti-based alloys were investigated as potential implant materials with focus on micro-alloying CP-Ti [49–51] and α-β Ti–6Al–4V with Cu [52–56]. Zhang et al. [49] have shown that the as-cast Ti–Cu alloys (with Cu < 10 wt.%) exhibit higher hardness and mechanical strength as well as a higher antibacterial rate (51–64%) but a relatively lower corrosion resistance than pure titanium. A problem is that excess copper content in an alloy can lead to material embrittlement, cytotoxicity [57], and in turn the binary Ti–Cu

Table 1 – Measured chemical compositions (in wt.% and at.%) and corresponding *e/a* ratios of the studied alloys.

Alloys (nominal composition)	Elemental content									e/a
	Ti		Nb		Ga		Cu		O	
	wt.%	at.%	wt.%	at.%	wt.%	at.%	wt.%	at.%	wt.%	
Ti–45Nb	55.44 (±0.17)	70.72	44.56 (±0.17)	29.28	\	\	\	\	0.09	4.29
$(Ti–45Nb)_{96}$-4Ga	52.37 (±0.33)	67.96	42.76 (±0.22)	28.59	3.87 (±0.04)	3.45	\	\	0.106 (±0.011)	4.25
$(Ti–45Nb)_{96}$-2Ga-2Cu	52.57 (±0.38)	67.84	42.96 (±0.22)	28.56	2.02 (±0.03)	1.79	1.95 (±0.03)	1.81	0.094 (±0.007)	4.21
$(Ti–45Nb)_{96}$–4Cu	52.30 (±0.53)	67.77	42.78 (±0.69)	28.56	\	\	3.76 (±0.28)	3.67	0.098 (±0.008)	4.18

alloys with reduced Cu cannot provide a high level β-phase stability, necessary for a low Young's modulus. The alloying of Cu to Ti can lead to the eutectoid transformation of β-Ti to α-Ti and tetragonal Ti_2Cu intermetallic compound, which explains why β-Ti is not commonly found in rapidly quenched TiCu-based alloys [58]. Therefore, there is a need for additional alloying elements to be introduced. Nb and Mo are suitable alloying additions for Ti-based alloys because they are well-known biocompatible β-stabilizers and can provide good mechanical properties and corrosion resistance [47,59–61]. Antibacterial β-type Ti-7.5Mo–5Cu and TNTZ-Cu_x alloys (x = 1–10 wt.%) were recently developed [47,51,58]. These Ti-based alloys exhibit an antibacterial function exerted by a controlled release of Cu ions, while maintaining a good corrosion resistance and biocompatibility. Hence, the Ti–Nb–Cu system is promising for developing β-Ti alloys with low elastic modulus and enhanced antibacterial properties. Some early studies on Ti–Nb–Cu alloys have been reported and they were mainly focused on structural and mechanical characteristics in view of developing shape-memory and superelastic alloys for biomedical applications [62]. Recently, Zhao et al. [63] investigated the corrosion and antibacterial properties of Ti–Nb–Cu alloys containing various Cu (0–3 wt.%) and Nb (0–30 wt.%) concentrations, and showed good bacterial inhibitory effect against *Staphylococcus aureus*.

Another fundamental property to be considered when developing metallic biomaterials is the corrosion resistance, as the metallic implant is dependent on the chemical interaction between the medical device and the surrounding biological environment. Corrosion can lead to the loss of structural integrity (with consequent implant failure), surface function and release of small amount of metal ions (e.g. Al, V), which might elicit adverse allergic reactions and even carcinogenesis [64]. The mentioned phenomena can be either prevented or inhibited by a surface with high passivation and re-passivation ability, which, in the case of titanium and its alloys, is a spontaneously developed passive, inert and stable film consisting mainly of TiO_2. The corrosion resistance of β-Ti alloys is generally higher when compared to α+β Ti alloys. However, corrosion resistance is also dependent on several factors such as environment, composition and microstructure. The influence of microstructure on corrosion resistance of biomedical implant alloys was investigated by Yu and Scully [65] on Ti–15Mo–3Nb–3Al. It was observed that the β solution-treated microstructure exhibits better corrosion resistance when compared to the aged one. The decrease in resistance of the aged sample was attributed to the partitioning of the alloying elements occurring during the aging process [66,67]. Therefore, composition and microstructural features strongly control the corrosion behavior of an alloy. Moreover, in β Ti–Nb alloys, the presence of Nb(V) ions contributes towards increasing the stability of the Ti(IV)-based passive film [68]. Previous investigations on the corrosion properties in Ringer's solution of a series of β Ti–Nb-based alloys showed low corrosion rates and stable anodic passivity in various physiological solutions [59,60]. The Ti–45Nb was chosen as starting composition due to its low Young's modulus (E ~ 65 GPa) in the solution-treated and quenched state [69] and to its high corrosion resistance [70].

The aim of the present study is to investigate the impact of alloying additions (up to 4 wt.%) of the antibacterial metallic elements Ga and Cu on microstructure, mechanical behavior and corrosion resistance of a Ti–45Nb alloy with the final scope of developing intrinsic antibacterial materials. Therefore, three novel single β-phase $(Ti–45Nb)_{96}$-4 Ga, $(Ti–45Nb)_{96}$–4Cu and $(Ti–45Nb)_{96}$-2 Ga–2Cu alloys were produced.

2. Materials and methods

2.1. Production of the alloys

High purity gallium (99.99%, purchased from *Haines & Maassen Metallhandelsgesellschaft mbH*) and high purity copper (99.9%, purchased from *Messinghaus Rehlken GmbH*) together with commercially available Ti–45Nb (wt.%, 99.9%, purchased from *ATI - Specialty Alloys & Components*, chemical composition is provided in Table 1) were used for the alloy preparation. Master alloys were manufactured with an arc-melter (*ALD Vacuum Technologies*) under a Ti-gettered argon atmosphere to bind eventual traces of oxygen. Button-shaped ingots were melted three times to ensure chemical homogeneity. The ingots were subsequently cast as cylindrical rods (Ø = 10 mm, length ~ 100 mm) in water-cooled molds with an in-house designed cold crucible device. In addition, alloying with Ga and/or Cu is effective in lowering the melting temperature of the Ti–Nb alloys (T_{mGa} = 29.8 °C, T_{mCu} = 1085 °C, T_{mTi-} = 1668 °C; T_{mNb} = 2468 °C) thus improving casting capability. For a homogenized microstructure without chemical segregations, the as-cast rods (encapsulated in argon-filled quartz tubes) were subjected to β-solution treatment at 1000 °C for 24 h. Subsequently, rods were water-quenched by breaking the tubes. For the present study, the developed alloys are compared with the commercially available Ti–45Nb alloy, itself subjected to the aforementioned solution-treatment.

2.2. Chemical composition analysis

The elemental composition of the solution-treated and quenched (STQ) alloys was checked by inductively coupled plasma optical emission spectroscopy (*iCAP 6500 Duo View, Thermo Fisher Scientific GmbH*) and possible contaminants (Si, Ta, Al < 0.1 wt% and Fe < 0.02 wt.%) were also scanned. Interstitial gas impurities such as oxygen and nitrogen were determined by the carrier gas hot extraction method (*LECO ON836, LECO Corporation*).

2.3. Material characterization

Microstructural studies were conducted by transmission X-ray diffraction (XRD) and scanning electron microscopy (SEM) analyses. Room temperature transmission XRD analysis was conducted using a *STOE Stadi P* diffractometer in transmission geometry using Mo $K_{\alpha 1}$ ($\lambda = 0.7093$ Å) monochromatic radiation at 50 kV and 30 mA. Diffraction patterns were recorded with a scan step of 0.010° and holding time of 90 s per step. Samples were prepared by mechanical grinding of a cross-section from the rod down to approximately 50 μm in thickness. Phase identification and analysis was carried out by Rietveld refinement [71], using *Malvern Panalytical's HighScore Plus*. Identification of crystalline phases is based on data from the International Centre of Diffraction Data (ICDD) PDF2 database (ICDD no-04-017-4957, bcc-Ti). Lattice parameters were determined by fitting the experimental patterns with *PseudoVoigt* function.

The microstructure of the developed alloys was studied by Scanning Electron Microscopy (SEM) equipped with an Energy Dispersive X-ray Spectrometer (EDX) and an Electron Backscattered Diffraction (EBSD) detector (*Zeiss Leo Gemini 1530*). Different elemental composition areas were detected in composition contrast mode (backscattered electrons) and analyzed with EDX analysis. EBSD maps for grain size determination were collected with a step size of 2 μm at magnification 50× and EBSD data were analyzed using ATEX software [72]. Specimen for SEM observations were sectioned from the rods and embedded in cold-hardening resin. Subsequently, the embedded samples were mechanically ground using SiC polishing sheets, followed by polishing using a colloidal suspension of SiO_2 (*OPS, Struers*) and finally cleaned ultrasonically with ethanol.

In order to assess the structural integrity of compression and tensile specimens, the latter were all scanned with a *2D GE Phoenix Nanotom M* X-ray absorption computed tomography (CT) device. No significant porosity was found in any of them.

2.4. Mechanical testing

Mechanical behavior of the alloys was investigated by tensile and compression tests as well as by microhardness measurement. Static uniaxial tensile tests were performed with a PC-controlled mini-tensile testing module DDS2-System (*Kammrath & Weiss GmbH*) equipped with a 5 kN load cell and a video-extensometer (controlled with *VEDDAC strain* software) under a constant strain rate of 3×10^{-4} s^{-1}. Flat dog-bone shaped tensile specimens with a total length of 14.67 mm (gauge length = 4.90 mm, width = 1.00 mm) were cut from the STQ rods and mechanically ground to 0.75 mm in thickness. Shape and size were designed according to the proportionality factor *k*, defined as the ratio between gauge length and square root of the cross section, of 5.65, as specified by the German standard for material testing (*DIN EN ISO 6892–1*). The following mechanical properties were determined from the engineering stress–strain curves: Young's modulus *E*, tensile yield strength σ_y^{tens} (proof offset 0.2%), ultimate tensile strength σ_{max} and maximum strain ε_{max}. At least three samples of each composition were tested. Uniaxial compression tests were carried out at room temperature using an *Instron 8562* testing device with a constant strain rate of 1.0×10^{-3} s^{-1}. Cylindrical specimens were prepared according to *DIN 50106:2016-11* with a height (6 mm) two times greater than the diameter (3 mm). Both loading surfaces were carefully polished (to be plane parallel) by wet grinding using silicon carbide papers. Plasticity and compression yield strength σ_y^{compr} (proof offset 0.2%) were determined from the curves. At least three repetitions per composition were performed. After the compression tests, the specimens were cut along the loading direction for further microstructural analyses such as XRD and EBSD to gain an understanding about the β phase stability post-deformation. Vickers microhardness ($HV_{0.1}$) measurements were conducted on polished, embedded samples using a Vickers microhardness tester (HMV-2, Shimadzu) with a force of 1 N (100 gf) and dwell time of 10 s. For each sample, at least 12 readings were collected at 12 chosen sites to reduce data scattering.

2.5. Corrosion studies

For the corrosion studies, circular electrodes with a thickness of 3 mm and diameter of 10 mm were cut from the rods and embedded in cold-hardening epoxy resin. The embedded samples were mechanically ground with P2500 silicon carbide emery paper and then cleaned in an ultrasonic bath of high purity ethanol. The exposed circular surface area of the investigated materials was estimated for each tested sample from optical micrographs using *ImageJ* software [73]. Right after the last grinding step, the sample is mounted into an in-house built rotating sample holder of appropriate diameter implemented in an Ametek (*Princeton Applied Research*) 616 B device activated with a very low rotation speed (50 rpm) and immersed in the testing solution. Rotation assists in the prevention of bubbles formation on the working electrode surface, which might cause unwanted fluctuations in the measured current. Measurements were started after ~0 min (several seconds). Electrochemical tests were carried out by means of a *Solartron SI 1287 Electrochemical* interface. A conventional three-electrode cell, with a jacket for temperature control, was assembled with a Pt net as counter electrode and a saturated calomel (SCE) as the reference electrode (E = 0.241 V vs. standard hydrogen electrode (SHE) at 25 °C). Measurements were conducted at 37.5 °C in air-saturated phosphate-buffered saline solution (PBS, pH ~ 7.4, composition: NaCl 140 mM, KCl 3 mM, phosphate buffer 10 mM, purchased from *Merck KGaA*), for which the pH was checked before and after every experiment.

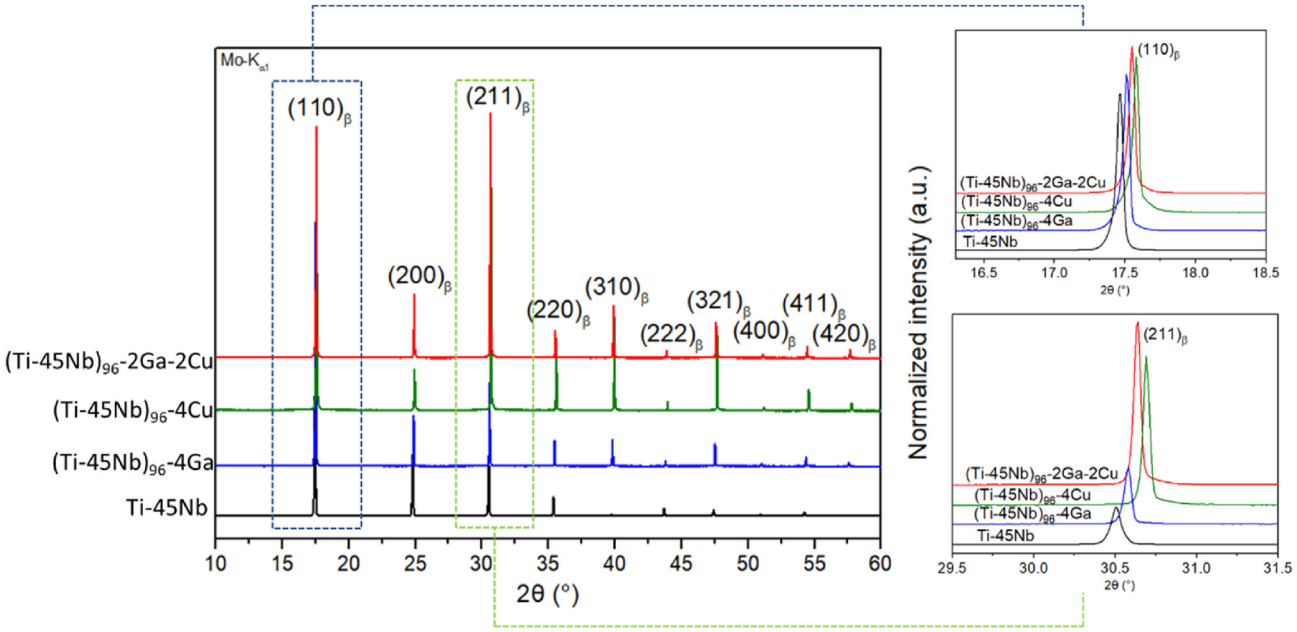

Fig. 1 – X-ray diffractograms of the developed alloys, together with the reference Ti–45Nb. Insets show the magnified view of the (110)$_\beta$ and (211)$_\beta$ diffraction peaks.

Before the actual polarization measurements, the samples were kept at open circuit potential (OCP) conditions for 4 h and the potential was monitored. OCP variations of less than 1 mV per minute were considered acceptable to start the polarization tests. The linear dynamic polarization was started at −0.2 V vs. OCP and increased with a constant sweep rate of 0.5 mV/s up to a value of +1 V vs. SCE. Each test was performed at least three times to verify the repeatability of the results. From the representative polarization curves, the characteristic corrosion parameters (E_{corr}, i_{corr} and average i_{pass} in the anodic potential range of +0.2 mV and +1.0 mV vs SCE.) were determined by graphical extrapolations. Stern–Geary equation [74] is used to determine the polarization resistance (R_p) after proper fitting of the curves.

2.6. *Statistical analysis*

All results are expressed as mean ± standard deviation from the multiple readings. One-factor ANOVA analyses, followed by multiple-comparison Tukey–Kramer post-hoc tests at $p = 0.05$, were done with *JASP* software [75]. A p-value < 0.05 is considered statistically significant, as indicated by an asterisk (*) in relevant figures.

3. Results

The present work investigates the microstructural, mechanical and chemical properties of three novel (Ti–45Nb)$_{96}$-4 Ga, (Ti–45Nb)$_{96}$-2 Ga–2Cu and (Ti–45Nb)$_{96}$–4Cu alloys. Chemical composition, including interstitial content of O and N, of the alloys, obtained by ICP-OES and CGHE analyses, is listed in Table 1. The measured nitrogen levels are below 0.0019 (±0.0002) wt.% and the oxygen levels are within the range of requirements specified as per ASTM F67 (CP–Ti grade 2, <0.25 wt.%) and of ASTM 4907 (Ti–6Al–4V ELI, < 0.13 wt.%). The measured oxygen contents in the range of 0.09–0.1 wt.% were lower than the threshold values that can deleteriously impact the ductility of Ti alloys [76]. Since the compositional changes were detected to be negligible, the three alloys are denoted by their nominal compositions. Based on the obtained compositions (in at.%), electron-per-atom ratio (e/a) was evaluated and listed in Table 1, which is a significant parameter influencing the β phase stability, and for the attainment of a lower modulus value for β-Ti alloys [77].

3.1. *Structural studies of the developed alloys*

Fig. 1 displays the X-ray diffraction patterns of the three developed alloys (Ti–45Nb)$_{96}$-4 Ga, (Ti–45Nb)$_{96}$-2 Ga–2Cu and (Ti–45Nb)$_{96}$–4Cu compared with the reference commercial alloy Ti–45Nb after solution-treatment at 1000 °C for 24 h and water quenching (STQ state). All the alloys displayed similar crystal structure belonging to the β-phase (space group: *Im-3m*) indicating that the elements are in complete solid solution with Ti and are capable of forming a metastable β phase at higher temperatures. No diffraction peaks belonging to secondary phases (α′, α″, ω) were observed. This can be attributed to the higher stabilizing effect of Nb on the parent β-phase and the higher cooling rates employed during casting. When Nb content is greater than 35 wt.%, a single β-phase is formed in Ti–Nb alloys [78]. As it is possible to notice from the magnified insets of (110) and (211) peaks (Fig. 1), only the β reflection appears, and no reflections were observed belonging to ω-phase (which might appear at lower angles) [79], α″-phase [9], or Cu–Ti intermetallic compounds in the two Cu-containing alloys, as previously reported for similar alloys [58]. Cubic bcc lattice constants determined by Rietveld refinement are

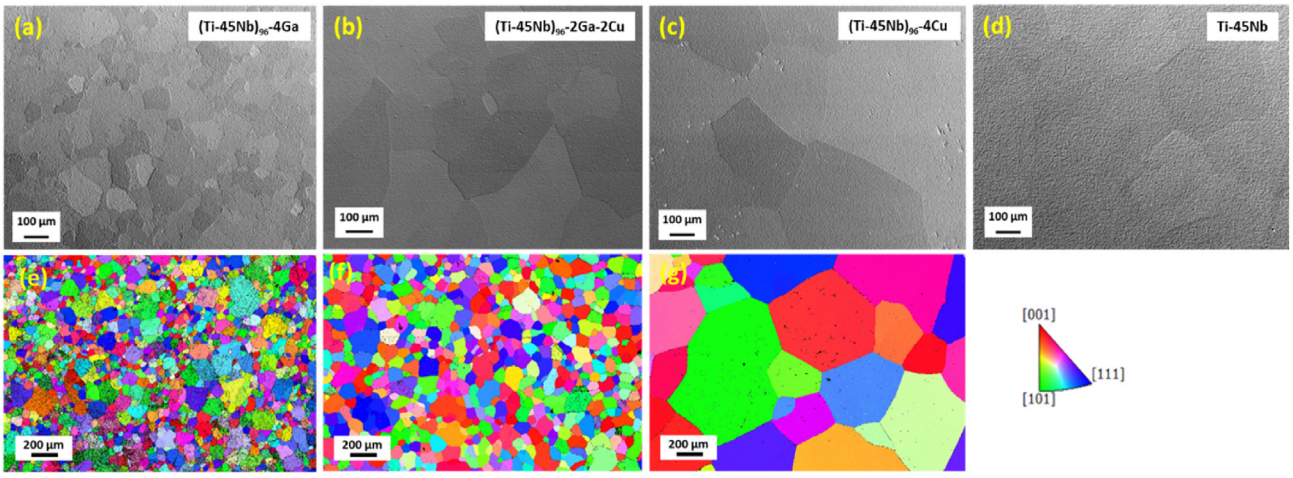

Fig. 2 – SEM micrographs and EBSD inverse pole figures (IPF) of polished cross-sectional regions of the alloys: (a,e) $(Ti–45Nb)_{96}$-4 Ga, (b,f) $(Ti–45Nb)_{96}$-2 Ga–2Cu, (c,g) $(Ti–45Nb)_{96}$–4Cu and (d) SEM micrograph of the reference Ti–45Nb alloy.

found to be in the range of 3.283–3.294 Å. An aspect to be pointed out is the peak shift towards higher angles, with a higher shift exhibited by $(Ti–45Nb)_{96}$–4Cu followed by $(Ti–45Nb)_{96}$-2 Ga–2Cu and $(Ti–45Nb)_{96}$-4 Ga: the addition of Ga and/or Cu resulted in a reduction in lattice constant compared to Ti–45Nb (a = 3.298 Å), pointing towards a solid solution strengthening effect.

The microstructures obtained after β-solutionizing and water-quenching are shown in Fig. 2a–d. All three alloys consist of equiaxed β-grains with various grain sizes. In addition, the EDX elemental mappings (Fig. 3) clearly depict the presence of chemically homogeneous microstructures for all the alloys without the presence of any micro-segregations. The average grain size (equivalent diameter) of the alloys $(Ti–45Nb)_{96}$-4 Ga, $(Ti–45Nb)_{96}$-2 Ga–2Cu and $(Ti–45Nb)_{96}$–4Cu were determined to be 55 μm, 90 μm and 323 μm based on EBSD mappings at 50× magnification, inverse pole figure (IPF) maps showing the β-grain orientations (Fig. 2e–g). This trend in grain size is also corroborated by the respective peak intensities in the XRD diffractograms, which increase in the same order: $(Ti–45Nb)_{96}$-4 Ga > $(Ti–45Nb)_{96}$-2 Ga–2Cu > $(Ti–45Nb)_{96}$–4Cu.

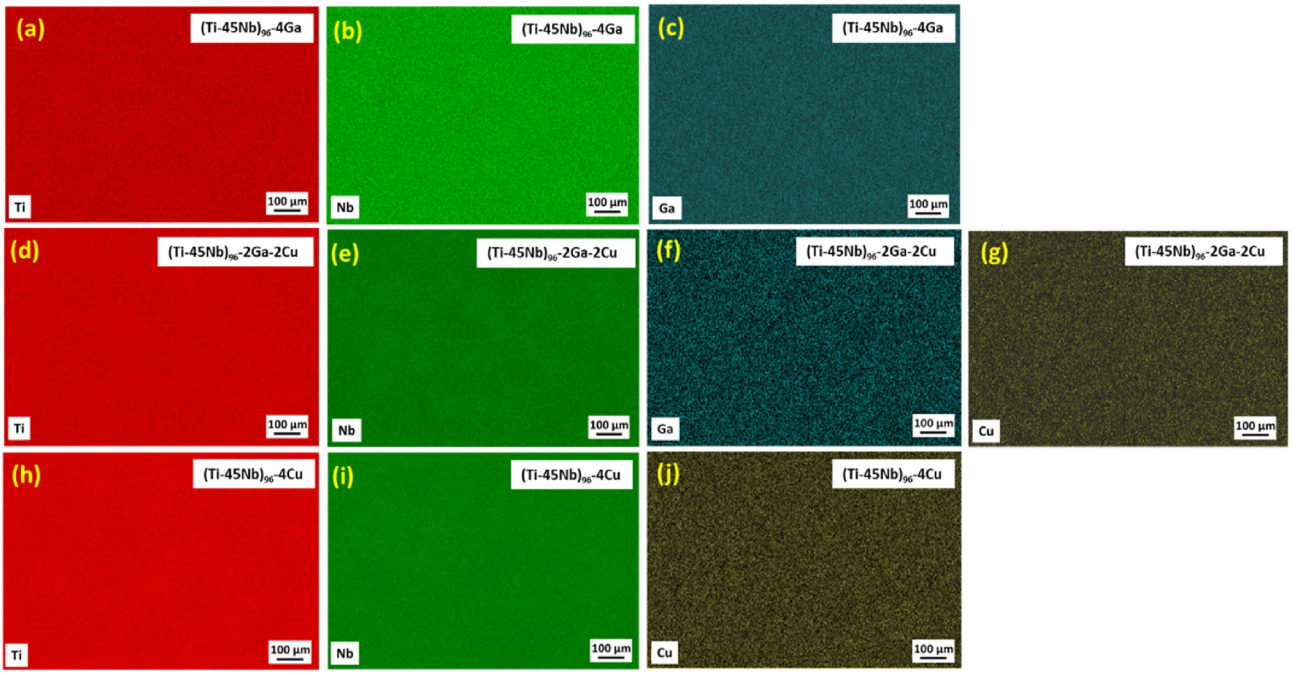

Fig. 3 – EDX mapping results of polished cross-sectional areas: (a–c) $(Ti–45Nb)_{96}$-4 Ga, (d–g) $(Ti–45Nb)_{96}$-2 Ga–2Cu and (h–j) $(Ti–45Nb)_{96}$–4Cu.

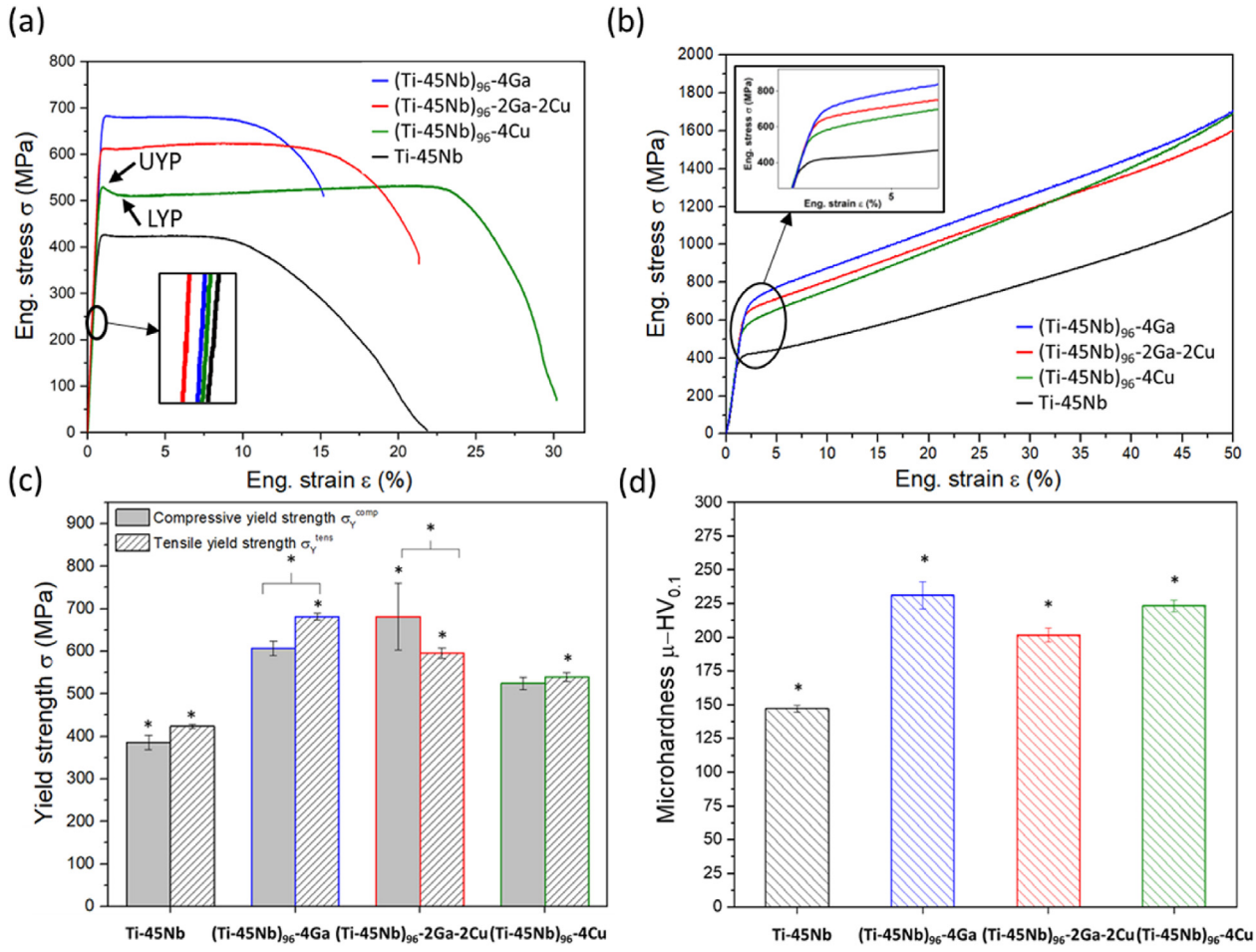

Fig. 4 – Engineering stress–strain curves of the three alloys and the reference Ti–45Nb in a) tension, b) compression, c) tensile and compressive yield strengths σ_Y and d) Vickers microhardness ($HV_{0.1}$). Significant comparisons are flagged (*).

3.2. *Mechanical analysis of the novel β alloys*

In order to evaluate the effect of Ga and/or Cu addition in terms of mechanical response, the mechanical behavior under both tensile and compressive loading was studied. Fig. 4a shows the tensile engineering stress–strain curves under *quasi*-static tensile load for the three alloys $(Ti–45Nb)_{96}$-4 Ga, $(Ti–45Nb)_{96}$-2 Ga–2Cu and $(Ti–45Nb)_{96}$–4Cu together with the reference Ti–45Nb. The resulting mechanical properties are listed in Table 2. The 0.2% offset yield strength values of $(Ti–45Nb)_{96}$-4 Ga, $(Ti–45Nb)_{96}$-2 Ga–2Cu and $(Ti–45Nb)_{96}$–4Cu are evaluated to be 681 (±8) MPa, 596 (±13) MPa and 539 (±10) MPa, respectively. An increase in yield strength of ~61% for $(Ti–45Nb)_{96}$-4 Ga, ~41% for $(Ti–45Nb)_{96}$-2 Ga–2Cu and ~27% for $(Ti–45Nb)_{96}$–4Cu is observed with respect to the reference Ti–45Nb. The measured Young's modulus, determined from the slope in the linear elastic region of the stress–strain curves, for the reference Ti–45Nb is 64.2 (±2.0) GPa, which is in good agreement with values reported in literature [24,80–82]. The addition of the alloying elements Ga and/or Cu to the Ti–Nb matrix led to a minor increase of *E* in the range of 73–78 GPa (Table 2), which falls

Table 2 – Mechanical properties of the investigated alloys in STQ state obtained from the engineering stress–strain curves of Fig. 4a: Young's modulus *E*, tensile yield strength σ^{tens} (0.2% proof stress), ultimate tensile strength σ_{max}, maximum tensile strain $\varepsilon^{tens}{}_{max}$, elastic energy δ_e, compressive yield strength σ^{comp}.

Alloys	Tensile tests					Compression tests
	E (GPa)	σ_Y^{tens} (MPa)	σ_{max} (MPa)	ε_{max} (%)	δ_e (MJ/m^3)	σ_Y^{comp} (MPa)
Ti–45Nb	64.2 ± 2.0	423 ± 5	426 ± 5	22 ± 2	1.90 ± 0.08	386 ± 17
$(Ti–45Nb)_{96}$-4Ga	77.7 ± 3.3	681 ± 8	675 ± 8	17 ± 2	3.67 ± 0.21	607 ± 17
$(Ti–45Nb)_{96}$-2Ga-2Cu	78.5 ± 2.5	596 ± 13	612 ± 11	22 ± 2	2.86 ± 0.09	681 ± 78
$(Ti–45Nb)_{96}$–4Cu	73.4 ± 1.9	539 ± 10	544 ± 10	28 ± 3	2.51 ± 0.05	525 ± 14

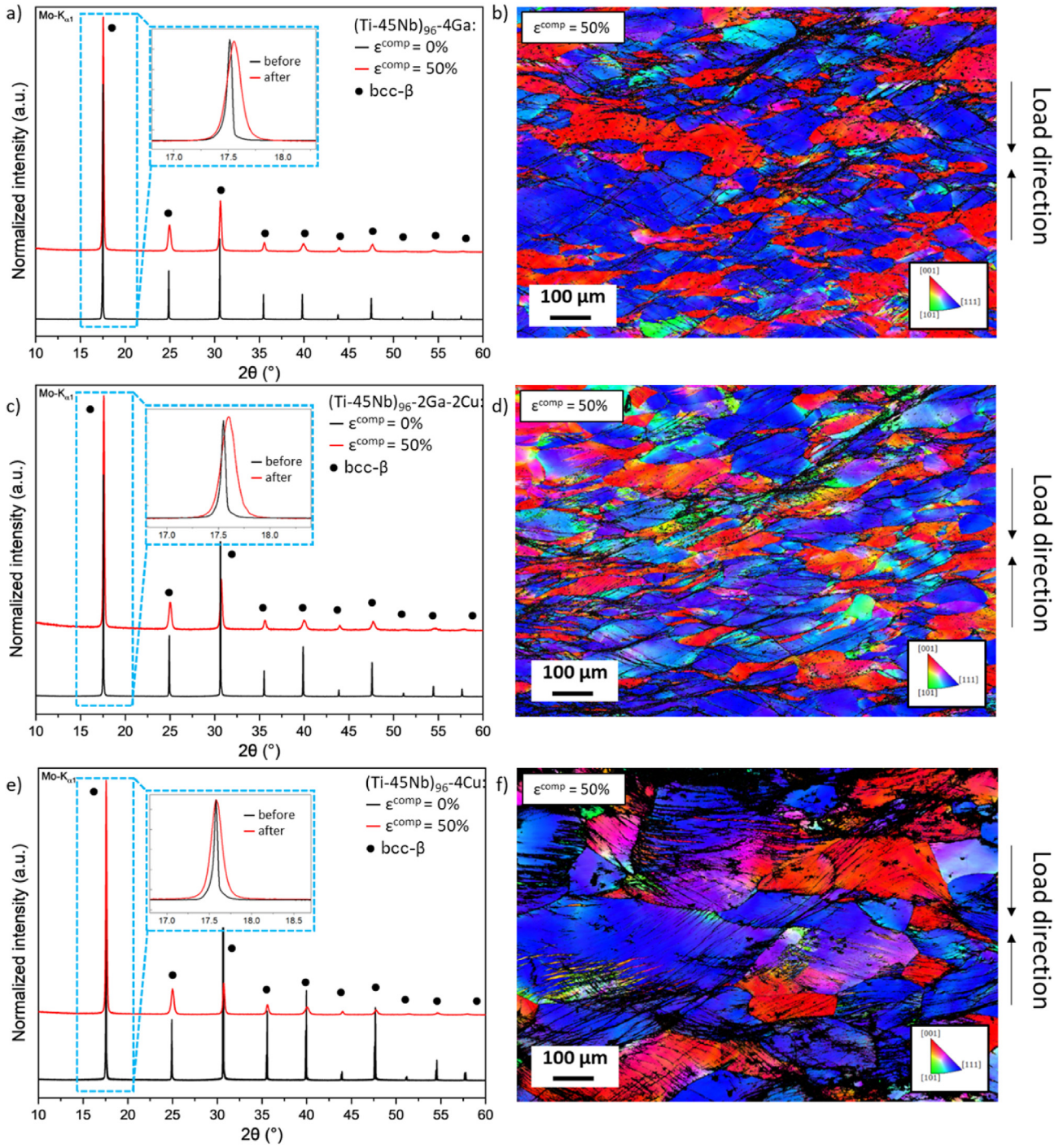

Fig. 5 – X-ray diffractograms of the three alloys (a, c, e) before (black line) and after (red line) compression test (compressive strain $\varepsilon^{comp.} = 50\%$). Insets show a magnification of the 2θ range between 17° and 19°. EBSD IPF maps (b, d, f) of the cross section of compressed specimens. Color coding is given with respect to the loading direction.

well within the criteria for required low modulus, as compared to conventional biomedical implant grades such as 316 L-stainless steel (205–210 GPa), Co–Cr alloys (220–230 GPa), CP-Ti (105 GPa), Ti–6Al–4V (110 GPa) and Ti–6Al–7Nb (105 GPa) [83]. All curves depict a distinct yield drop from the well-defined upper yield point (UYP) to the lower yield point (LYP), which is more pronounced for $(Ti–45Nb)_{96}$–4Cu alloy, as indicated in Fig. 4a. A similar phenomenon, attributed to strain aging arising from the diffusion of solute atoms (e.g. N, C, Zn, Mg) to temporarily arrested dislocations, has been observed in other alloys: mild steels [84], Al–Mg alloys [85], Cu–Zn alloys [86] and Ti–Nb-based gum metals [58,79,87]. In addition, the developed alloys display improved values of engineering strains (ε_{max}) of 17% for $(Ti–45Nb)_{96}$-4 Ga, 22% for $(Ti–45Nb)_{96}$-2 Ga–2Cu and 28% for $(Ti–45Nb)_{96}$–4Cu. As it can be inferred from the obtained

Table 3 – The lattice parameter of bcc-phase determined by Rietveld method before and after compression tests, together with the full width at half maximum (FWHM) of the first diffraction peak.

Alloy	Experimental bcc lattice constant (Å)		FWHM of $(110)_\beta$ (rad·10^3)		
	Initial state	After compression ($\varepsilon^{comp.} = 50\%$)	Initial state	After compression ($\varepsilon^{comp.} = 50\%$)	Increase (%)
$(Ti–45Nb)_{96}$-4Ga	3.294	3.284	1.356	2.429	79%
$(Ti–45Nb)_{96}$-2Ga-2Cu	3.289	3.280	0.763	2.812	269%
$(Ti–45Nb)_{96}$–4Cu	3.283	3.277	0.819	3.000	266%

stress–strain curves (Fig. 4a), the specimens uniformly deform and elongate prior to necking, the latter starting at very large strains, in the order 4 Ga < 2 Ga–2Cu < 4Cu. In all the curves, it is possible to observe a long plateau with limited work hardening after yield drop, which is more pronounced for the Cu-bearing alloy. This behavior is similar to a Lüders plateau found in mild steel, which consists of a single band of plastic deformation traveling along the specimen [84]. The elastic energy (δ_e) was calculated by analyzing the area under the tensile stress–strain curves in the elastic regime [24], values are reported in Table 2 and increase in the order: $(Ti–45Nb)_{96}$-4 Ga > $(Ti–45Nb)_{96}$-2 Ga–2Cu > $(Ti–45Nb)_{96}$–4Cu. The compressive engineering stress–strain curves are reported in Fig. 4b. The stopping criterion for the compressive tests was 50% of samples' height reduction, as the samples displayed no fracture with even high strains up to 75% (*not shown here*), for this reason fracture strengths are not reported in Table 2. All alloys displayed very large plastic strains (exceeding 50%), indicating an excellent workability. A significant increase in the compressive yield strengths compared to the reference Ti–45Nb can also be observed. Tensile and compressive yield strengths of the alloys are shown in Fig. 4c and listed in Table 2. Asymmetry in yield strength determined from compression and tension testing is reported for many Ti-based alloys in literature [88–90]. The average Vickers microhardness (μ-$HV_{0.1}$) values of Ti–45Nb, $(Ti–45Nb)_{96}$-4 Ga, $(Ti–45Nb)_{96}$-2 Ga–2Cu and $(Ti–45Nb)_{96}$–4Cu are found to be 147 (±3), 231 (±10), 202 (±5) and 223 (±4) HV, respectively (Fig. 4d). All the three developed alloys displayed microhardness values greater than 200 HV with almost 37–57% increase as compared to the reference Ti–45Nb.

3.3. *β-phase stability after high compressive strains*

The compression stress–strain curves show a conspicuous strain hardening, but no double yielding effect originating from the formation of stress-induced α''-martensite [91]. In order to gain more insights into the influence of compressive

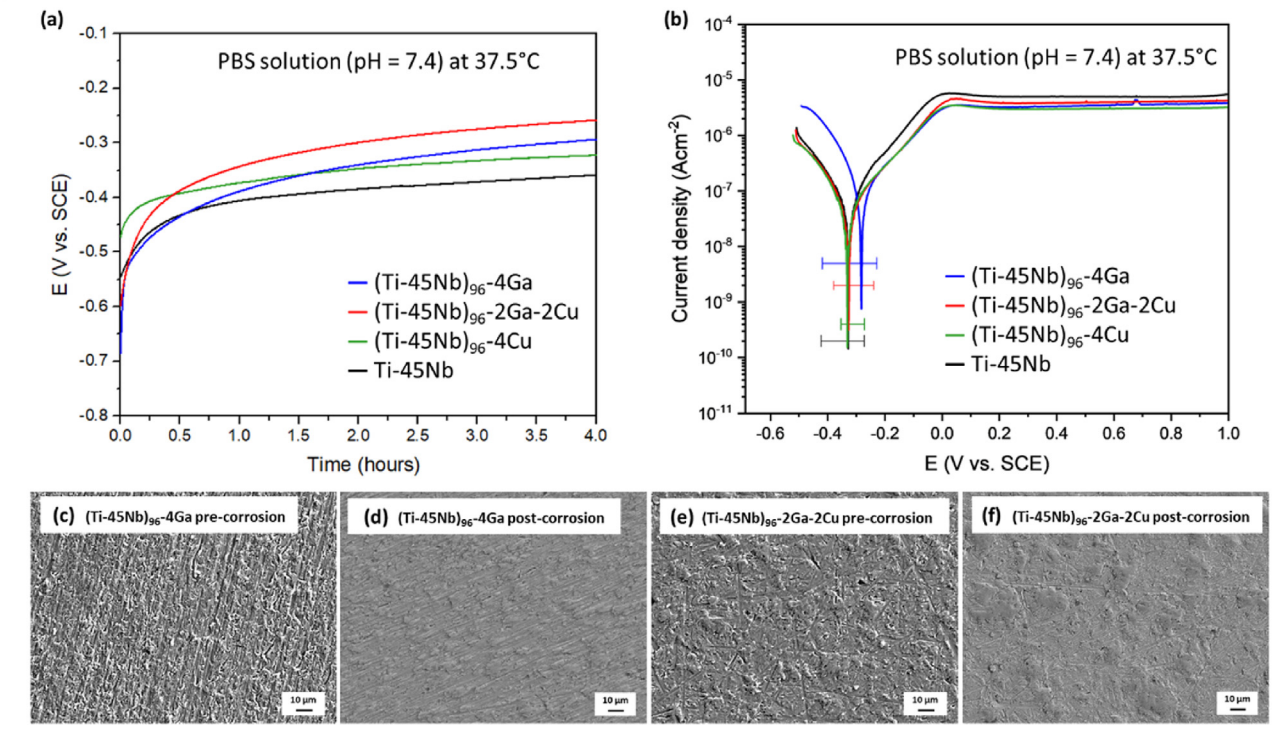

Fig. 6 – Corrosion tests in PBS solution (pH = 7.4) at 37.5 °C: (a) open circuit potentials (OCP) during 4 h of immersion, (b) linear anodic polarization curves collected at a scan rate of 0.5 mV/s, (c–f) representative SEM micrographs of the alloys $(Ti–45Nb)_{96}$-4 Ga, $(Ti–45Nb)_{96}$-2 Ga–2Cu before and after corrosion test in PBS at 37.5 °C.

Table 4 – Electrochemical parameters extrapolated from the OCP curves and potentiodynamic polarization curves: open-circuit potential (E_{OCP}), corrosion potential (E_{corr}), corrosion current density (i_{corr}), average passive current density (i_{pass}) at the anodic potential range of +0.2 mV and +1.0 mV vs SCE, polarization resistance (R_p). Potential values are reported vs SCE (E = + 0.241 V).

Alloys	E_{OCP} (mV)	E_{corr} (mV)	i_{corr} (nA cm^{-2})	i_{pass} (μA cm^{-2})	R_p (kΩ cm^2)
Ti–45Nb	−346 ± 68	−348 ± 76	80 ± 20	4.0 ± 1.1	387 ± 93
$(Ti–45Nb)_{96}$-4Ga	−342 ± 37	−360 ± 59	88 ± 24	4.5 ± 1.5	315 ± 82
$(Ti–45Nb)_{96}$-2Ga-2Cu	−286 ± 56	−305 ± 65	64 ± 13	4.2 ± 0.3	382 ± 130
$(Ti–45Nb)_{96}$–4Cu	−307 ± 28	−312 ± 41	69 ± 16	3.7 ± 0.7	383 ± 99

strains on the β-phase stability of the alloys, heavily deformed compression specimens (~50% in height reduction) were cross-sectioned along the loading direction for further structural analyses. X-ray diffractograms before and after compression tests are shown in Fig. 5a,c,e. In all patterns of the heavily deformed samples, no other peaks apart the ones exclusively indexed with cubic bcc (*Im-3m*) are detectable, indicating that the parent β-phase is fully retained. It is possible to observe a broadening of the peaks, because of the residual compressive stresses in the microstructure, and a shift to higher angles because of the shrinkage of the lattice constants achieved by compressive deformation (Table 3). The changes in the peak intensities suggest a development of the crystallographic texture with deformation. These results were further confirmed by EBSD analyses (Fig. 5b,d,f), which show heavily deformed and elongated β-grains due to the uniaxial compressive loading. Crystal orientations are indicated by an RGB mixture. Most of the areas in the shown maps correspond to a preferred orientation of $[110]_\beta$ (in blue), in bcc systems, where the slip direction is always in <111>.

3.4. *Corrosion behavior in PBS solution*

With the scope of simulating the inorganic composition of blood, electrochemical corrosion studies were conducted at 37.5 °C in PBS solution, which closely mimics osmolarity and physiological pH (~7.4) of tissue cells. The explored potential region (−0.5 V to +1 V vs SCE) of the Ti-based alloy working electrodes is of interest when developing materials for implant applications [62]. Fig. 6a shows the open circuit potential (OCP) evolution (potential vs. time) of the alloys under investigation during 4 h of immersion time. After reaching near-steady OCP conditions, anodic polarization tests at low scan rate (*quasi*-static conditions) were conducted and representative curves are displayed in Fig. 6b. Relevant electrochemical parameters are listed in Table 4. OCP curves show a potential increase over time, which indicates the formation of a protective passive mixed oxide layer on the surface. Initially, right after mechanically grinding and immersion in the electrolyte solution, E_{ocp} values are in the range of −750 to −450 mV vs SCE, reflecting very reactive surfaces. E_{ocp} values, which have reached a stable plateau regime after approximately 40–45 min, gradually increase (ΔE < 1 mV/min), ending in the range of −450 to −250 mV vs SCE. Following the E_{ocp} measurements, linear polarization tests were conducted immediately. Considering the limitations of the method, the electrochemical response of all developed alloys is very similar to that of the reference Ti–45Nb. The alloys show, in the linear polarization curves (Fig. 6b), very low corrosion rates, in the range of 64–88 nA/cm^2 and transfer in the anodic regime into a stable plateau referring to the passive state without any sign of pitting. The average passive current density, measured in the range +0.2 mV and 1.0 mV vs SCE, is rather low, in the range of 3.7–4.5 μA/cm^2. Overall, the polarization behavior is very similar to (Ti–40Nb)–4In alloy reported by Gebert et al. [59], where they observed corrosion current densities of only 0.1–0.2 μA/cm^2 and passive current densities of 3–4 μA/cm^2, without any indication of pitting. In this passive potential range up to +1 V vs SCE, mainly a thermodynamically stable mixed Ti(IV)- and Nb(V)-based oxide forms onto the anodically polarized alloys [92]. Nb was previously shown to have a beneficial effect on the corrosion stability and passivation property of Ti-based alloys by decreasing the concentration of anion vacancies in the passive film [68,70,93,94]. Experimental values are in good agreement with those reported for similar alloys, in particular a Ti–45Nb alloy tested in artificial saliva [81]. Moreover, the developed alloys show higher corrosion resistance if compared to the clinically used Ti–6Al–4V [95]. No significant difference could be detected among studied alloys, meaning that the strong passivating nature of the valve metals Ti and Nb dominates the entire corrosion behavior of the alloys in the explored potential region. Surface of the working electrode was observed before and after the corrosion tests: a similar morphology can be observed in the SEM micrographs; representative images are shown (Fig. 6 c-f). The smoother surface visible after the test is very likely due to the electrochemically-induced growth of the oxide layer. No signs of corrosion products are visible, in accordance with the electrochemical measurements. Similar observations were made for the other alloys (Fig. S1). Micro-alloying of the elements Cu and Ga does not significantly affect corrosion resistance of the TiNb-based alloys.

4. Discussion

The major objective of the present study was to develop novel β-type Ti alloys with antibacterial elemental addition (Ga and/or Cu) while maintaining a low Young's modulus value, which can be achieved via a retained β phase. The two antibacterial metallic elements have distinctive effects on Ti phase transformation ($Ti^{\alpha\rightarrow\beta} = 882$ °C): Ga is an α-stabilizer, whereas Cu is an eutectoid β-stabilizer [58]. In order to assess the β phase stability, molybdenum equivalent criterion $[Mo]_{eq}$ represents one of the useful parameters and is generally used to design

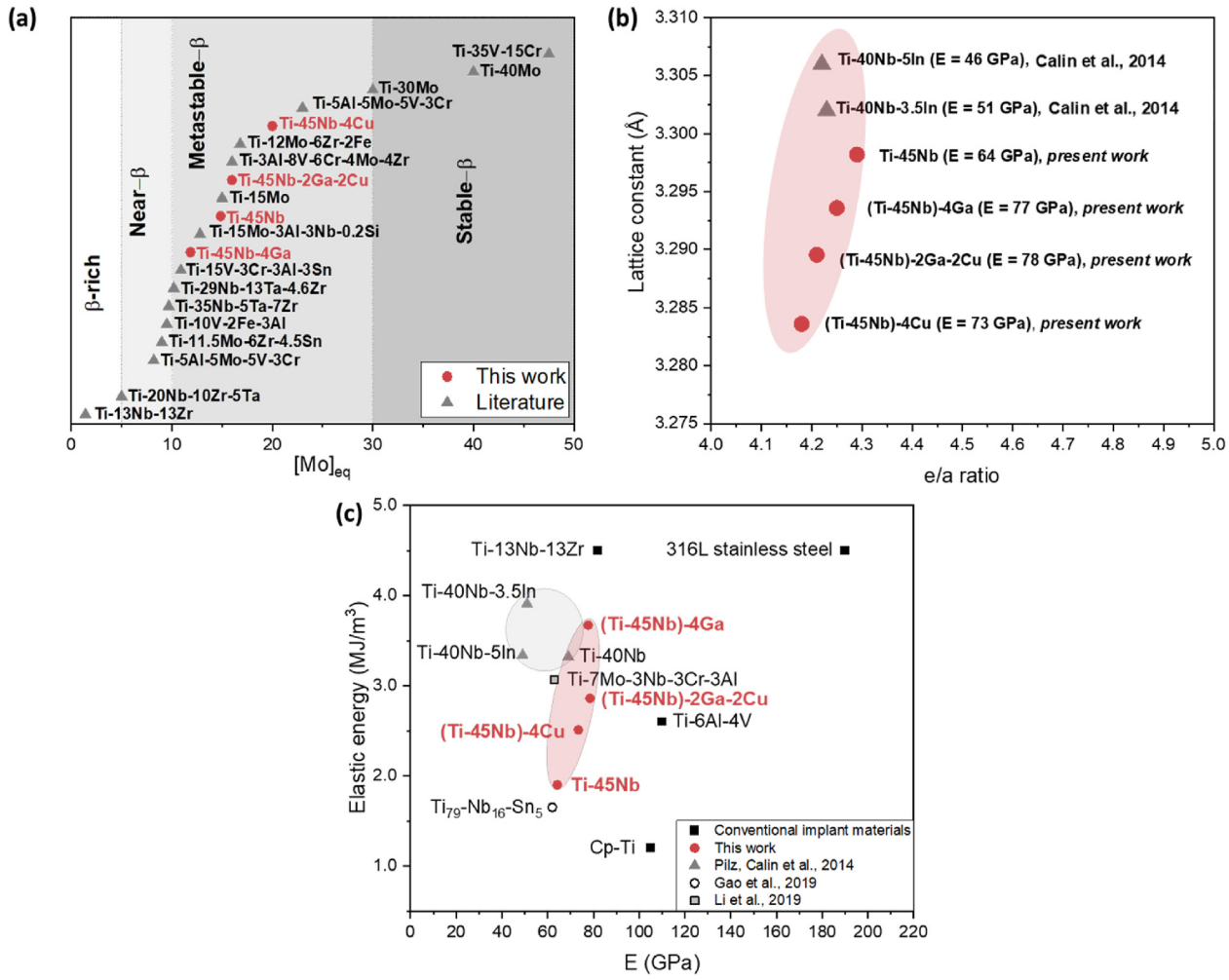

Fig. 7 – (a) Distribution of $[Mo]_{eq}$ showing the β phase stability of the developed alloys compared with other β Ti alloys [100,101]; b) Obtained cubic lattice parameter plotted vs electron-per-atom ratio (*e/a*) compared with similar alloys in literature; (c) Variation of elastic energy with Young's modulus *E* compared with other relevant implant materials for load bearing applications.

many β Ti alloys. $[Mo]_{eq}$ can be determined with the following equation (Eqn (1)), in which the equivalent contribution of elements towards β-stabilizing capacity compared to the strong stabilizer Mo is provided. For the alloy design in the present study, an updated expression of $[Mo]_{eq}$ reported by Jiang et al. [96] has been used, in which the coefficient for Nb is modified, taking into consideration its stronger β stabilization ability. Since Ga is an α-stabilizer (the highest solubility of Ga in β-Ti is 27 at.% at 1420 °C [97]), its tendency to stabilize the α phase in a β matrix is also incorporated in the expression for $[Al]_{eq}$, for which the coefficient is taken as 0.5, based on the works of Shamblen and Redden [98]. While Cu, according to the Cu–Ti binary phase diagram and relevant literature [49,58,99], is a β-eutectoid stabilizer with limited solubility in Ti (17.2 wt.% in β-Ti at 990 °C); Cu forms, by eutectoid reaction, the intermetallic compound Ti_2Cu [56] and hence has a higher coefficient of 1.51. In addition, the minor concentration of interstitial O and N, capable of drastically affecting the β phase stability, has been taken into consideration by maintaining it in the composition range of about 0.1 wt.%.

$$[Mo]_{eq} = [Mo] + 0.25[Ta] + 0.33[Nb] + 0.59[W] + 1.25[V] + 1.84[Cr] + 2.46[Ni] + 1.93[Fe] + 1.51[Cu] + 2.67[Co] + 2.26[Mn] + 0.3[Sn] + 0.31[Zr] + 3.01[Si] - 1.47[Al] \quad (1)$$

$$[Al]_{eq} = 1[Al] + 0.5[Ga] + 10[O+N] \quad (2)$$

The alloys in the present study, $(Ti–45Nb)_{96}$-4 Ga, $(Ti–45Nb)_{96}$-2 Ga–2Cu and $(Ti–45Nb)_{96}$–4Cu were designed based on the $[Mo]_{eq}$ values of 11.85, 15.97 and 19.98 respectively, which fall within the range of metastable β Ti alloys capable of retaining β phase during solution-treatment (Fig. 7a).

The electron per atom ratio (*e/a*) ratio is another widely used theoretical parameter in the design of low modulus β Ti alloys. A regular pattern can be observed for a physical property variation against *e/a* ratio, and anomalies in this regular pattern indicate electronic structural changes within the alloy matrix [102]. Experimentally obtained β lattice constant values are plotted with respect to the *e/a* ratio in Fig. 7b together with data from literature. It can be deduced that the developed

alloys fall within the region of *e/a* ratios for which similar Ti–Nb-based alloys exhibit low E values. Physical property such as Young's modulus *E* is a direct consequence of interatomic interactions and electronic states, which are obviously affected by the presence of alloying elements [87]. This could be explained keeping into account the different atomic sizes of the alloying elements Ti, Nb, Ga and Cu, whose atomic radii are 1.46 Å, 1.43 Å, 1.39 Å and 1.28 Å, respectively [103]. This is also evident from the difference in the calculated lattice constants (Table 3), which are smaller as compared to pure Ti. Lattice constants are similar to those reported for Ti–Nb binary alloys [104], Ti–Nb–Zr–Sn and Ti–Nb–Zr–Sn–Mo alloys [101,105]. The replacement of Ti and Nb with the smaller atoms Cu and Ga brings the alloying atoms closer in the β crystal lattice, in agreement with the smaller lattice constants reported in Fig. 7b, and thus *E* increases by 15–20% compared with reference Ti–45Nb. However, *E* of developed alloys is in the range 73 ÷ 78 GPa, which is way lower (30–44%) than the values of the clinically used Ti–6Al–4V ASTM grade 5 ($E = 114$ GPa) or CP-Ti grade 2 ($E = 105$ GPa).

As previously reported, with a Nb content greater than 30 wt.%, a single bcc β-phase Ti-based solid solution can be obtained by quenching [69]. Despite the addition Ga and Cu, the combination of the enhanced β-stabilizing effect of Nb and the high cooling rates achieved during casting resulted in full retainment of single bcc β-phase for the three alloys, as demonstrated by the XRD results (Fig. 1) [6]. In addition, formation of Ti_2Cu precipitate was prevented in the two Cu-bearing alloys. Solution-treatment above β-transus resolved micro-segregations formed during the casting process and lead to a homogeneous distribution (Fig. 3) of the alloying elements within the solid solution. X-ray diffraction patterns are well consistent with those for similar alloys, as reported by Lee et al. on a series of cast Ti–Nb alloys [78], Bönisch et al. [9] on Ti–Nb alloys, Lai et al. [79] on Ti–Nb-based gum metals. All alloys display well-developed equiaxed β-grains with significantly different grain sizes. Grain size values are in good agreement with those reported in literature for β-Ti alloys in solution-treated and quenched state [25,106]. The grain refinement observed for the Ga-bearing alloy might be due to a reduced atomic mobility, that slows down grain growth during the casting and subsequent solution-treatment. A similar effect of Ga as grain refiner was observed on the microstructure of Mg- and Pb-based alloys [107–109]. In the investigated alloys, grain boundary strengthening and solid-solution strengthening induce an obstruction to the dislocation motion during plastic deformation, thereby contributing towards the improved strength. Increase in strength with reduction in grain size is clearly evident from the tensile test results. The presence of the alloying elements Ga and Cu also improved microhardness, as shown in Fig. 4d, values are in good agreement with those reported for similar β-type alloys with a dominant β phase matrix [80,81]. It can be clearly deduced that the presence of the alloying elements Ga and/or Cu renders a significant strengthening effect.

The underlying hardening mechanism arising from the increased dislocation density is also evident from the broadening of XRD peaks after compression as shown in insets (Fig. 5a,c,e). In addition, the difference in atomic size of the alloying elements Ga and Cu compared with Ti and Nb might be a conceivable factor affecting yield strength, more pronounced in the case of Ga. The substitutional solid solution hardening phenomenon occurs due to the addition of solute elements with smaller atomic radius. As discussed above, the replacement of Ti and Nb with the ~ 3–10% smaller atoms of Cu and Ga brings the alloying atoms closer in bcc crystal lattice, corroborating the smaller observed lattice constants, thereby contributing towards an increase in strength. None of the alloys showed signs of cracking or fracture in compression, implying that the presence of the alloying element atoms is not deleterious to plasticity, which is high for all alloys. Calin et al. [24] tested in compression a series of (Ti–40Nb)-xIn alloys and also observed similar values in yield strength and excellent plasticity. The alloys in this work displayed low work hardening and no continuous yielding in the engineering tensile stress–strain curves. The plasticity in tension of the three alloys was also not reduced by alloying with Cu and Ga when compared to the reference Ti–45Nb. Fig. 7c shows the elastic energy as a function of the Young's modulus for a series of commercial implant materials and Ti alloys in literature. Values for the three alloys range between 2.51 ÷ 3.67 MJ/m^3 and are higher than those of Cp-Ti. The Ga-bearing alloy exhibits the highest value, significantly higher than Ti–6Al–4V, indicating greater bearing of elastic deformation. For β-type Ti–Nb alloys, deformation twinning is generally observed for Nb content up to 42 wt.% (at room temperature) [23], however the dominant deformation mode changes from twinning to dislocation slip in alloys with high β stability [110], which is indeed the case for the alloys in the present work. Microstructural investigations on highly compressed samples ($\varepsilon^{comp.} = 50\%$) confirm this aspect, where a single β phase was retained. Nevertheless twinning, which is known to increase strain hardening in β-Ti alloys [111], cannot be totally excluded, because the presence of twins might be hindered by the deformation bands formed during the compression tests (Fig. 5b,d,f). Therefore, further investigations at lower strains are needed to clarify this aspect. These results are in good agreement with previous studies on the deformation mechanism in a heavily stabilized β-type (Ti–40Nb)-3.5In [25]. Even after thermo-mechanical processing (hot and cold rolling with various thickness reduction), no sign of deformation-induced phase transformation was observed for these In-containing β-Ti alloys [25]. Similar results were obtained by Sadeghpour et al. [20] for a heavily stabilized β-type Ti-based alloy (Ti–3Al–8Mo–7V–3Cr, wt.%) deformed at low strain rates, where the deformation mechanism was attributed to only slip, further confirmed by XRD and EBSD analyses [22,23].

Corrosion properties in synthetic physiological conditions were also evaluated by OCP monitoring and linear anodic polarization measurements in *quasi*-static conditions. Results reveal that the corrosion resistance of the developed alloys is high in PBS solution at 37.5 °C, indicating that the presence of small additions of the alloying elements Ga and Cu is not deleterious. However detailed studies on the presence of antibacterial elements Ga and Cu in the surface passive film and on their eventual release kinetics in physiological conditions need further exploration. According to the traditional

electrochemical equilibria diagrams of the pure alloying elements in water at 25 °C, these metals spontaneously passivate at explored physiological pH (7.4). Due to the wide passivity range of these alloys, a similar behavior can also be expected at other possible physiological pH conditions such as during surgery (pH 5.6) and in case of infection conditions (pH 9.0). Reducing the pH value towards more acidic, below 5, could result in an enhanced release of antibacterial ions, due to the breakdown of the oxide films [112]. These results are similar to the previous investigations on a (Ti–40Nb)–4In alloy, which exhibits very low corrosion rates and stable anodic passivity in synthetic physiological fluids [59]. In that case too, In was homogeneously dissolved in the β-phase matrix with no detectable effect on the electrochemical response.

5. Conclusions

The present work investigated the microstructural characteristics, mechanical response and corrosion aspects of three novel (Ti–45Nb)-based alloys containing small amounts (up to 4 wt.%) of the alloying elements Ga and Cu, namely: $(Ti–45Nb)_{96}$-4 Ga, $(Ti–45Nb)_{96}$–4Cu and $(Ti–45Nb)_{96}$-2 Ga–2Cu, designed based on $[Mo]_{eq}$ and electron-per-atom (e/a) ratio. Ga and Cu were chosen because of their outstanding inherent antibacterial and antibiofilm properties, which render these alloys suitable to be used to tackle antibiotic-resistant implant-associated infections. The findings from this study can be summarized as follows:

- All three alloys in STQ state display a single bcc β-phase microstructure with a homogeneous microstructure devoid of any elemental segregation. The observed microstructures suggest that small additions of Ga lead to improved grain refinement, as compared to Cu addition.
- All alloys show higher yield strengths (in compression 31–55%, and tension 24–47%) and higher elastic energy (28–64%) than the reference Ti–45Nb. The highest tensile strain of 28 (±3) % was recorded for the $(Ti–45Nb)_{96}$–4Cu alloy. Young's modulus of the alloys is in the range 73 ÷ 79 GPa, which is lower than clinically-used alloys.
- Microhardness also increases (32–44%) with Ga and/or Cu addition. These observations were mainly attributed to solid solution and grain boundary strengthening.
- β-phase is observed to be stable even after high compressive strains with no other deformation-induced phases (at $\varepsilon^{comp} = 50\%$). Dislocation slip is the main dominant deformation mechanism in the three alloys.
- Small additions of the alloying elements Ga and Cu do not deleteriously affect the corrosion resistance of the alloys in the explored potential region and pH.

All three alloys could potentially be used for advanced structural and biomedical applications. Desired bactericidal properties might be exerted by either ion release or contact killing, further investigations in this sense are progressing. As a whole, this study suggests that the $(Ti–45Nb)_{96}$-4 Ga alloy exhibits a great balance in terms of low stiffness, high strength, ductility and high corrosion resistance.

Funding information

L.A.A., M.C. and A.G. are grateful for the financial support from the European Commission within the H2020-MSCA grant agreement No. 861046 (BIOREMIA-ITN). A.H. and A.G. acknowledge for funding within the OsteoLas project, partially financed by the European Regional Development Fund (EFRE) and by tax revenues on the basis of the budget adopted by the Members of the Parliament of Saxony (funding reference 100382989). S.P. and A.G. acknowledge for funding the Deutsche Forschungsgemeinschaft (DFG) under project GE/1106/12–1 (no 419952351). The publication of this article was funded by the Open Access Fund of the Leibniz Association.

Declaration of Competing Interest

The authors declare that they have no known competing financial interests or personal relationships that could have appeared to influence the work reported in this paper.

Acknowledgments

The authors are grateful to Andrea Voβ for chemical analysis and to D. Seifert, H. Buβkamp, K. Baumgart and D. Sven for the technical assistance. Stimulating discussions with J. Freudenberger are gratefully acknowledged.

Appendix A. Supplementary data

Supplementary data to this article can be found online at https://doi.org/10.1016/j.jmrt.2022.08.111.

REFERENCES

[1] Long M, Rack HJ. Titanium alloys in total joint replacement—a materials science perspective. Biomaterials 1998;19(18):1621–39. https://doi.org/10.1016/S0142-9612(97)00146-4.
[2] Sarraf M, Rezvani Ghomi E, Alipour S, Ramakrishna S, Liana Sukiman N. A state-of-the-art review of the fabrication and characteristics of titanium and its alloys for biomedical applications. Bio-Design Manuf 2022;5:371–95. https://doi.org/10.1007/s42242-021-00170-3.
[3] Inan-Eroglu E, Ayaz A. Is aluminum exposure a risk factor for neurological disorders? J Res Med Sci 2018;23:51. https://doi.org/10.4103/jrms.JRMS_921_17.
[4] Gomes CC, Moreira LM, Santos VJSV, Ramos AS, Lyon JP, Soares CP, et al. Assessment of the genetic risks of a metallic alloy used in medical implants. Genet Mol Biol 2011;34:116–21. https://doi.org/10.1590/S1415-47572010005000118.
[5] Ridzwan MIZ, Shuib S, Hassan AY, Shokri AA, Mohammad Ibrahim MN. Problem of stress shielding and improvement to the hip implant designs: a review. J Med Sci 2007;7:460–7. https://doi.org/10.3923/jms.2007.460.467.
[6] Ozaki T, Matsumoto H, Watanabe S, Hanada S. Beta Ti alloys with low young's modulus. Mater Trans 2004;45:2776–9. https://doi.org/10.2320/matertrans.45.2776.

[7] Kim HY, Miyazaki S. Several issues in the development of Ti–Nb-based shape memory alloys. Shape Mem Superelasticity 2016;2:380–90. https://doi.org/10.1007/s40830-016-0087-7.
[8] Kim HY, Hashimoto S, Kim J Il, Hosoda H, Miyazaki S. Mechanical properties and shape memory behavior of Ti-Nb alloys. Mater Trans 2004;45:2443–8. https://doi.org/10.2320/matertrans.45.2443.
[9] Bönisch M, Panigrahi A, Stoica M, Calin M, Ahrens E, Zehetbauer M, et al. Giant thermal expansion and α-precipitation pathways in Ti-alloys. Nat Commun 2017;8:1429. https://doi.org/10.1038/s41467-017-01578-1.
[10] Bönisch M, Calin M, Waitz T, Panigrahi A, Zehetbauer M, Gebert A, et al. Thermal stability and phase transformations of martensitic Ti–Nb alloys. Sci Technol Adv Mater 2013;14:055004. https://doi.org/10.1088/1468-6996/14/5/055004.
[11] Kwak TY, Yang JY, Heo YB, Kim SJ, Kwon SY, Kim WJ, et al. Additive manufacturing of a porous titanium layer structure Ti on a Co-Cr alloy for manufacturing cementless implants. J Mater Res Technol 2021;10:250–67. https://doi.org/10.1016/j.jmrt.2020.11.080.
[12] Zhuravleva K, Bönisch M, Prashanth KG, Hempel U, Helth A, Gemming T, et al. Production of porous β-type Ti-40Nb alloy for biomedical applications: comparison of selective laser melting and hot pressing. Materials 2013;6:5700–12. https://doi.org/10.3390/ma6125700.
[13] Li YH, Shang XY. Recent progress in porous TiNb-based alloys for biomedical implant applications. Mater Sci Technol 2020;36:385–92. https://doi.org/10.1080/02670836.2020.1724415.
[14] Xu W, Lu X, Hayat MD, Tian J, Huang C, Chen M, et al. Fabrication and properties of newly developed Ti35Zr28Nb scaffolds fabricated by powder metallurgy for bone-tissue engineering. J Mater Res Technol 2019;8:3696–704. https://doi.org/10.1016/j.jmrt.2019.06.021.
[15] Ohyama H, Nishimura T. Effects of alloying elements on deformation mode in Ti-V based β titanium alloy system. ISIJ Int 1995;35:927–36. https://doi.org/10.2355/isijinternational.35.927.
[16] Song Y, Xu DS, Yang R, Li D, Wu WT, Guo ZX. Theoretical study of the effects of alloying elements on the strength and modulus of β-type bio-titanium alloys. Mater Sci Eng, A 1999;260:269–74. https://doi.org/10.1016/s0921-5093(98)00886-7.
[17] Ou KL, Weng CC, Lin YH, Huang MS. A promising of alloying modified beta-type Titanium-Niobium implant for biomedical applications: microstructural characteristics, in vitro biocompatibility and antibacterial performance. J Alloys Compd 2017;697:231–8. https://doi.org/10.1016/j.jallcom.2016.12.120.
[18] Sun J, Yao Q, Xing H, Guo WY. Elastic properties of β, α″ and ω metastable phases in Ti-Nb alloy from first-principles. J Phys Condens Matter 2007;19. https://doi.org/10.1088/0953-8984/19/48/486215.
[19] Kolli RP, Joost WJ, Ankem S. Phase stability and stress-induced transformations in beta titanium alloys. JOM (J Occup Med) 2015;67:1273–80. https://doi.org/10.1007/s11837-015-1411-y.
[20] Sadeghpour S, Javaheri V, Bruschi S, Kömi J, Karjalainen P. Strain rate and mechanical stability in determining deformation behavior of beta Ti alloys. Mater Sci Eng, A 2020;798. https://doi.org/10.1016/j.msea.2020.140274.
[21] Sadeghpour S, Abbasi SM, Morakabati M, Kisko A, Karjalainen LP, Porter DA. On the compressive deformation behavior of new beta titanium alloys designed by d-electron method. J Alloys Compd 2018;746:206–17. https://doi.org/10.1016/j.jallcom.2018.02.212.
[22] Hanada S, Ozeki M, Izumi O. Deformation characteristics in B phase Ti-Nb alloys. Metall Trans A 1985;16:789–95. https://doi.org/10.1007/BF02814829.
[23] Hanada S, Yoshio T, Izumi O. Effect of plastic deformation modes on tensile properties of beta titanium alloys. Trans Japan Inst Met 1986;27:496–503. https://doi.org/10.2320/matertrans1960.27.496.
[24] Calin M, Helth A, Gutierrez Moreno JJ, Bönisch M, Brackmann V, Giebeler L, et al. Elastic softening of β-type Ti-Nb alloys by indium (In) additions. J Mech Behav Biomed Mater 2014;39:162–74. https://doi.org/10.1016/j.jmbbm.2014.07.010.
[25] Pilz S, Geissler D, Calin M, Eckert J, Zimmermann M, Freudenberger J, et al. Thermomechanical processing of In-containing β-type Ti-Nb alloys. J Mech Behav Biomed Mater 2018;79:283–91. https://doi.org/10.1016/j.jmbbm.2017.12.028.
[26] Souza JGS, Bertolini MM, Costa RC, Nagay BE, Dongari-Bagtzoglou A, Barão VAR. Targeting implant-associated infections: titanium surface loaded with antimicrobial. iScience 2021;24. https://doi.org/10.1016/j.isci.2020.102008.
[27] Ghilini F, Pissinis DE, Miñán A, Schilardi PL, Diaz C. How functionalized surfaces can inhibit bacterial adhesion and viability. ACS Biomater Sci Eng 2019;5:4920–36. https://doi.org/10.1021/acsbiomaterials.9b00849.
[28] Hayama AOF, Andrade PN, Cremasco A, Contieri RJ, Afonso CRM, Caram R. Effects of composition and heat treatment on the mechanical behavior of Ti-Cu alloys. Mater Des 2014;55:1006–13. https://doi.org/10.1016/j.matdes.2013.10.050.
[29] Yumak N, Aslantaş K. A review on heat treatment efficiency in metastable β titanium alloys: the role of treatment process and parameters. J Mater Res Technol 2020;9. https://doi.org/10.1016/j.jmrt.2020.10.088.
[30] Cochis A, Azzimonti B, Della Valle C, Chiesa R, Arciola CR, Rimondini L. Biofilm formation on titanium implants counteracted by grafting gallium and silver ions. J Biomed Mater Res, Part A 2015;103:1176–87. https://doi.org/10.1002/jbm.a.35270.
[31] Goss CH, Kaneko Y, Khuu L, Anderson GD, Ravishankar S, Aitken ML, et al. Gallium disrupts bacterial iron metabolism and has therapeutic effects in mice and humans with lung infections. Sci Transl Med 2018;10:1–12. https://doi.org/10.1126/scitranslmed.aat7520.
[32] Kaneko Y, Thoendel M, Olakanmi O, Britigan BE, Singh PK. The transition metal gallium disrupts Pseudomonas aeruginosa iron metabolism and has antimicrobial and antibiofilm activity. J Clin Invest 2007;117:877–88. https://doi.org/10.1172/JCI30783.
[33] Rzhepishevska O, Ekstrand-Hammarström B, Popp M, Björn E, Bucht A, Sjöstedt A, et al. The antibacterial activity of Ga3+ is influenced by ligand complexation as well as the bacterial carbon source. Antimicrob Agents Chemother 2011;55:5568–80. https://doi.org/10.1128/AAC.00386-11.
[34] Verron E, Masson M, Khoshniat S, Duplomb L, Wittrant Y, Baud'Huin M, et al. Gallium modulates osteoclastic bone resorption in vitro without affecting osteoblasts. Br J Pharmacol 2010;159:1681–92. https://doi.org/10.1111/j.1476-5381.2010.00665.x.
[35] Chitambar CR. Gallium-containing anticancer compounds. Future Med Chem 2012;4:1257–72.
[36] Qiu KJ, Lin WJ, Zhou FY, Nan HQ, Wang BL, Li L, et al. Ti-Ga binary alloys developed as potential dental materials. Mater Sci Eng C 2014;34:474–83. https://doi.org/10.1016/j.msec.2013.10.004.
[37] Bumgardner JD, Johansson BI. Galvanic corrosion and cytotoxic effects of amalgam and gallium alloys coupled to

titanium. Eur J Oral Sci 1996;104:300–8. https://doi.org/10.1111/j.1600-0722.1996.tb00081.x.
[38] Cochis A, Azzimonti B, Chiesa R, Rimondini L, Gasik M. Metallurgical gallium additions to titanium alloys demonstrate a strong time-increasing antibacterial activity without any cellular toxicity. ACS Biomater Sci Eng 2019;5:2815–20. https://doi.org/10.1021/acsbiomaterials.9b00147.
[39] Inamura T, Fukui Y, Hosoda H, Wakashima K, Miyazaki S. Mechanical properties of Ti-Nb biomedical shape memory alloys containing Ge or Ga. Mater Sci Eng C 2005;25:426–32. https://doi.org/10.1016/j.msec.2005.01.025.
[40] Hosoda H, Fukui Y, Inamura T, Wakashima K, Miyazaki S. Mechanical properties of Ti-Nb biomedical shape memory alloys containing 13- and 14-group elements. Mater Sci Forum 2005;475–479:2329–32. https://doi.org/10.4028/www.scientific.net/msf.475-479.2329.
[41] Uauy R, Olivares M, Gonzalez M. Essentiality of copper in humans. Am J Clin Nutr 1998;67:952–9. https://doi.org/10.1093/ajcn/67.5.952S.
[42] Gallo J, Holinka M, Moucha CS. Antibacterial surface treatment for orthopaedic implants, vol. 15; 2014. https://doi.org/10.3390/ijms150813849.
[43] Liu R, Memarzadeh K, Chang B, Zhang Y, Ma Z, Allaker RP, et al. Antibacterial effect of copper-bearing titanium alloy (Ti-Cu) against Streptococcus mutans and Porphyromonas gingivalis. Sci Rep 2016;6:1–10. https://doi.org/10.1038/srep29985.
[44] Li M, Ma Z, Zhu Y, Xia H, Yao M, Chu X, et al. Toward a molecular understanding of the antibacterial mechanism of copper-bearing titanium alloys against Staphylococcus aureus. Adv Healthc Mater 2016;5:557–66. https://doi.org/10.1002/adhm.201500712.
[45] Konieczny J, Rdzawski Z. Antibacterial properties of copper and its alloys Related papers Inexpensive mineral copper mat erials wit h ant ibact erial surfaces Antibacterial properties of copper and its alloys the creation of Educational and Scientific Centre of Railway Transport. Arch Mater Sci Eng 2012:53–60.
[46] Liu J, Li F, Liu C, Wang H, Ren B, Yang K, et al. Effect of Cu content on the antibacterial activity of titanium-copper sintered alloys. Mater Sci Eng C 2014;35:392–400. https://doi.org/10.1016/j.msec.2013.11.028.
[47] Xu D, Wang T, Wang S, Jiang Y, Wang Y, Chen Y, et al. Antibacterial effect of the controlled nanoscale precipitates obtained by different heat treatment schemes with a Ti-based nanomaterial, Ti–7.5Mo–5Cu alloy. ACS Appl Bio Mater 2020;3:6145–54. https://doi.org/10.1021/acsabm.0c00716.
[48] Ren L, Ma Z, Li M, Zhang Y, Liu W, Liao Z, et al. Antibacterial properties of Ti-6Al-4V-xCu alloys. J Mater Sci Technol 2014;30:699–705. https://doi.org/10.1016/j.jmst.2013.12.014.
[49] Zhang E, Wang X, Chen M, Hou B. Effect of the existing form of Cu element on the mechanical properties, bio-corrosion and antibacterial properties of Ti-Cu alloys for biomedical application. Mater Sci Eng C 2016;69:1210–21. https://doi.org/10.1016/j.msec.2016.08.033.
[50] Wu JH, Chen KK, Chao CY, Chang YH, Du JK. Effect of Ti2Cu precipitation on antibacterial property of Ti-5Cu alloy. Mater Sci Eng C 2020;108. https://doi.org/10.1016/j.msec.2019.110433.
[51] Fowler L, Masia N, Cornish LA, Chown LH, Engqvist H, Norgren S, et al. Development of antibacterial Ti-Cux alloys for dental applications: effects of ageing for alloys with up to 10 wt% cu. Materials 2019;12:1–13. https://doi.org/10.3390/ma12234017.
[52] Ma Z, Ren L, Liu R, Yang K, Zhang Y, Liao Z, et al. Effect of heat treatment on Cu distribution, antibacterial performance and cytotoxicity of Ti-6Al-4V-5Cu alloy. J Mater Sci Technol 2015;31:723–32. https://doi.org/10.1016/j.jmst.2015.04.002.
[53] Sherif ESM, Abdo HS, Latief FH, Alharthi NH, Abedin SZ El. Fabrication of Ti-Al-Cu new alloys by inductive sintering, characterization, and corrosion evaluation. J Mater Res Technol 2019;8:4302–11. https://doi.org/10.1016/j.jmrt.2019.07.040.
[54] Koike M, Cai Z, Oda Y, Hattori M, Fujii H, Okabe T. Corrosion behavior of cast Ti-6Al-4V alloyed with Cu. J Biomed Mater Res Part B Appl Biomater 2005;73:368–74. https://doi.org/10.1002/jbm.b.30225.
[55] Wang S, Ma Z, Liao Z, Song J, Yang K, Liu W. Study on improved tribological properties by alloying copper to CP-Ti and Ti-6Al-4V alloy. Mater Sci Eng C 2015;57:123–32. https://doi.org/10.1016/j.msec.2015.07.046.
[56] Akbarpour MR, Mirabad HM, Hemmati A, Kim HS. Processing and microstructure of Ti-Cu binary alloys: a comprehensive review. Prog Mater Sci 2022;127:100933. https://doi.org/10.1016/j.pmatsci.2022.100933.
[57] Lemire JA, Harrison JJ, Turner RJ. Antimicrobial activity of metals: mechanisms, molecular targets and applications. Nat Rev Microbiol 2013;11:371–84. https://doi.org/10.1038/nrmicro3028.
[58] Fowler L, van Vuuren AJ, Goosen W, Engqvist H, Öhman-Mägi C, Norgren S. Investigation of copper alloying in a TNTZ-Cux alloy. Materials 2019;12:1–13. https://doi.org/10.3390/ma12223691.
[59] Gebert A, Oswald S, Helth A, Voss A, Gostin PF, Rohnke M, et al. Effect of indium (In) on corrosion and passivity of a beta-type Ti-Nb alloy in Ringer's solution. Appl Surf Sci 2015;335:213–22. https://doi.org/10.1016/j.apsusc.2015.02.058.
[60] Pilz S, Gebert A, Voss A, Oswald S, Göttlicher M, Hempel U, et al. Metal release and cell biological compatibility of beta-type Ti-40Nb containing indium. J Biomed Mater Res Part B Appl Biomater 2018;106:1686–97. https://doi.org/10.1002/jbm.b.33976.
[61] Godley R, Starosvetsky D, Gotman I. Corrosion behavior of a low modulus β-Ti-45%Nb alloy for use in medical implants. J Mater Sci Mater Med 2006;17:63–7. https://doi.org/10.1007/s10856-006-6330-6.
[62] Horiuchi Y, Nakayama K, Inamura T, Kim HY, Wakashima K, Miyazaki S, et al. Effect of Cu addition on shape memory behavior of Ti-18 mol%Nb alloys. Mater Trans 2007;48:414–21. https://doi.org/10.2320/matertrans.48.414.
[63] Zhao Z, Xu W, Xin H, Yu F. Microstructure, corrosion and anti-bacterial investigation of novel Ti-xNb-yCu alloy for biomedical implant application. J Mater Res Technol 2022:118159. https://doi.org/10.1016/j.jmrt.2022.04.158.
[64] Niinomi M. Metals for biomedical devices. 2010. https://doi.org/10.1533/9781845699246.
[65] Yu SY, Scully JR. Corrosion and passivity of Ti-13% Nb-13% Zr in comparison to other biomedical implant alloys. Corrosion 1997;53.
[66] Yu SY, Brodrick CW, Ryan MP, Scully JR. Effects of Nb and Zr alloying additions on the activation behavior of Ti in hydrochloric acid. J Electrochem Soc 1999;146:4429–38. https://doi.org/10.1149/1.1392655.
[67] Sarma J, Kumar R, Sahoo AK, Panda A. Enhancement of material properties of titanium alloys through heat treatment process: a brief review. Mater Today Proc 2020;23:561–4. https://doi.org/10.1016/j.matpr.2019.05.409.
[68] Metikoš-Huković M, Kwokal A, Piljac J. The influence of niobium and vanadium on passivity of titanium-based implants in physiological solution. Biomaterials

2003;24:3765–75. https://doi.org/10.1016/S0142-9612(03)00252-7.
[69] Hanada S, Ozaki T, Takahashi E, Watanabe S, Yoshimi K, Abumiya T. Composition dependence of Young's modulus in beta titanium binary alloys. Mater Sci Forum 2003;426–432:3103–8. https://doi.org/10.4028/www.scientific.net/msf.426-432.3103.
[70] Gostin PF, Helth A, Voss A, Sueptitz R, Calin M, Eckert J, et al. Surface treatment, corrosion behavior, and apatite-forming ability of Ti-45Nb implant alloy. J Biomed Mater Res Part B Appl Biomater 2013;101B:269–78. https://doi.org/10.1002/jbm.b.32836.
[71] Young RA. The Rietveld method. 1993.
[72] Fundenberger J-J, Beausir B. ATEX software - analysis tools for electron and X-ray diffraction. 2017.
[73] Rasband WS. ImageJ, U. S. National Institutes of Health, Bethesda, Maryland, USA [n.d].
[74] Metikoš-Huković M, Zevnik C. Determination of Polarization resistance and corrosion rate by using pulse method, polarization curves and AAS. Mater Corros 1982;33:661–8. https://doi.org/10.1002/maco.19820331204.
[75] JASP team. JASP 2020., Version 0.14.1.
[76] Zhao D, Chang K, Ebel T, Qian M, Willumeit R, Yan M, et al. Microstructure and mechanical behavior of metal injection molded Ti-Nb binary alloys as biomedical material. J Mech Behav Biomed Mater 2013;28:171–82. https://doi.org/10.1016/j.jmbbm.2013.08.013.
[77] Abdel-Hady M, Hinoshita K, Morinaga M. General approach to phase stability and elastic properties of β-type Ti-alloys using electronic parameters. Scripta Mater 2006;55:477–80. https://doi.org/10.1016/j.scriptamat.2006.04.022.
[78] Lee CM, Ju CP, Chern Lin JH. Structure-property relationship of cast Ti-Nb alloys. J Oral Rehabil 2002;29:314–22. https://doi.org/10.1046/j.1365-2842.2002.00825.x.
[79] Lai MJ, Tasan CC, Raabe D. Deformation mechanism of ω-enriched Ti-Nb-based gum metal: dislocation channeling and deformation induced ω-β transformation. Acta Mater 2015;100:290–300. https://doi.org/10.1016/j.actamat.2015.08.047.
[80] Thoemmes A, Ivanov IV, Ruktuev AA, Lazurenko DV, Bataev IA. Structure and phase composition of biomedical alloys of the Ti – Nb system in cast condition and after heat treatment. Met Sci Heat Treat 2019;60:659–65. https://doi.org/10.1007/s11041-019-00334-0.
[81] Bai Y, Deng Y, Zheng Y, Li Y, Zhang R, Lv Y, et al. Characterization, corrosion behavior, cellular response and in vivo bone tissue compatibility of titanium-niobium alloy with low Young's modulus. Mater Sci Eng C 2016;59:565–76. https://doi.org/10.1016/j.msec.2015.10.062.
[82] Hon Y, Wang J, Pan Y. Composition/phase structure and properties of titanium-niobium alloys. Mater Trans 2003;44:2384–90.
[83] Navarro M, Michiardi A, Castaño O, Planell JA. Biomaterials in orthopaedics. J R Soc Interface 2008;5:1137–58. https://doi.org/10.1098/rsif.2008.0151.
[84] Ananthakrishna G. Current theoretical approaches to collective behavior of dislocations. Phys Rep 2007;440:113–259. https://doi.org/10.1016/j.physrep.2006.10.003.
[85] Aboulfadl H, Deges J, Choi P, Raabe D. Dynamic strain aging studied at the atomic scale. Acta Mater 2015;86:34–42. https://doi.org/10.1016/j.actamat.2014.12.028.
[86] Ardley GWR, Cottrell AHS. Yield points in brass crystals. Proc R Soc London Ser A Math Phys Sci 1953;219:328–40.
[87] Saito T, Furuta T, Hwang JH, Kuramoto S, Nishino K, Suzuki N, et al. Multifunctional alloys obtained via a dislocation-free plastic deformation mechanism. Science 2003;300:464–7. https://doi.org/10.1126/science.1081957. 80-.
[88] Gao P, Fan J, Sun F, Cheng J, Li L, Tang B, et al. Crystallography and asymmetry of tensile and compressive stress-induced martensitic transformation in metastable β titanium alloy Ti–7Mo–3Nb–3Cr–3Al. J Alloys Compd 2019;809. https://doi.org/10.1016/j.jallcom.2019.151762.
[89] Syed FW, Anil Kumar V, Gupta RK, Kanjarla AK. Role of microstructure on the tension/compression asymmetry in a two-phase Ti-5Al-3Mo-1.5V titanium alloy. J Alloys Compd 2019;795:151–62. https://doi.org/10.1016/j.jallcom.2019.04.272.
[90] Neeraj T, Savage MF, Tatalovich J, Kovarik L, Hayes RW, Mills MJ. Observation of tension-compression asymmetry in α/β and titanium alloys. Philos Mag A 2005;85:279–95. https://doi.org/10.1080/14786430412331315707.
[91] Elmay W, Prima F, Gloriant T, Bolle B, Zhong Y, Patoor E, et al. Effects of thermomechanical process on the microstructure and mechanical properties of a fully martensitic titanium-based biomedical alloy. J Mech Behav Biomed Mater 2013;18:47–56. https://doi.org/10.1016/j.jmbbm.2012.10.018.
[92] Vishnu J, Ansheed AR, Hameed P, Praveenkumar K, Pilz S, Alberta LA, et al. Insights into the surface and biocompatibility aspects of laser shock peened Ti-22Nb alloy for orthopedic implant applications. Appl Surf Sci 2022;586:152816. https://doi.org/10.1016/j.apsusc.2022.152816.
[93] Kobayashi E, Wang TJ, Doi H, Yoneyama T, Hamanaka H. Mechanical properties and corrosion resistance of Ti-6Al-7Nb alloy dental castings. J Mater Sci Mater Med 1998;9:567–74. https://doi.org/10.1023/A:1008909408948.
[94] Helth A, Gostin PF, Oswald S, Wendrock H, Wolff U, Hempel U, et al. Chemical nanoroughening of Ti40Nb surfaces and its effect on human mesenchymal stromal cell response. J Biomed Mater Res Part B Appl Biomater 2014;102:31–41. https://doi.org/10.1002/jbm.b.32976.
[95] Benea L, Simionescu-Bogatu N. Reactivity and corrosion behaviors of Ti6Al4V alloy implant biomaterial under metabolic perturbation conditions in physiological solutions. Materials 2021;14:7404. https://doi.org/10.3390/ma14237404.
[96] Jiang B, Wang Q, Wen D, Xu F, Chen G, Dong C, et al. Effects of Nb and Zr on structural stabilities of Ti-Mo-Sn-based alloys with low modulus. Mater Sci Eng, A 2017;687:1–7. https://doi.org/10.1016/j.msea.2017.01.047.
[97] Antonova NV, Tretyachenko LA. Phase diagram of the Ti-Ga system. J Alloys Compd 2001;317–318:398–405. https://doi.org/10.1016/S0925-8388(00)01416-X.
[98] Shamblen CE, Redden TK. Creep resistance and high-temperature metallurgical stability of titanium alloys containing gallium. OR Trans 1972;3:1299–305. https://doi.org/10.1007/BF02642464.
[99] The Materials Information Society. ASM handbook volume 3 - alloy phase diagrams. 1992. https://doi.org/10.1007/BF02869318.
[100] Kolli RP, Devaraj A. A review of metastable beta titanium alloys. Metals (Basel) 2018;8:1–41. https://doi.org/10.3390/met8070506.
[101] Kent D, Wang G, Dargusch M. Effects of phase stability and processing on the mechanical properties of Ti-Nb based β Ti alloys. J Mech Behav Biomed Mater 2013;28:15–25. https://doi.org/10.1016/j.jmbbm.2013.07.007.
[102] Tiwari GP, Ramanujan RV. Relation between the electron to atom ratio and some properties of metallic systems. J Mater Sci 2001;36:271–83. https://doi.org/10.1023/A:1004853304704.

[103] Senkov ON, Miracle DB. Effect of the atomic size distribution on glass forming ability of amorphous metallic alloys. Mater Res Bull 2001;36:2183–98. https://doi.org/10.1016/S0025-5408(01)00715-2.
[104] Kim HY, Ikehara Y, Kim JI, Hosoda H, Miyazaki S. Martensitic transformation, shape memory effect and superelasticity of Ti-Nb binary alloys. Acta Mater 2006;54:2419–29. https://doi.org/10.1016/j.actamat.2006.01.019.
[105] Hao YL, Li SJ, Sun SY, Yang R. Effect of Zr and Sn on Young's modulus and superelasticity of Ti-Nb-based alloys. Mater Sci Eng, A 2006;441:112–8. https://doi.org/10.1016/j.msea.2006.09.051.
[106] Helth A, Pilz S, Kirsten T, Giebeler L, Freudenberger J, Calin M, et al. Effect of thermomechanical processing on the mechanical biofunctionality of a low modulus Ti-40Nb alloy. J Mech Behav Biomed Mater 2017;65:137–50. https://doi.org/10.1016/j.jmbbm.2016.08.017.
[107] Mohedano M, Blawert C, Yasakau KA, Arrabal R, Matykina E, Mingo B, et al. Characterization and corrosion behavior of binary Mg-Ga alloys. Mater Char 2017;128:85–99. https://doi.org/10.1016/j.matchar.2017.03.040.
[108] Nazri SF, Salleh MAAM. The effects of gallium additions on the microstructure of lead-free solder materials: a short review. Solid State Phenom 2018;280:187–93. https://doi.org/10.4028/www.scientific.net/SSP.280.187.
[109] Hernández-Cortés AA, Escobedo-Bocardo JC, Cortés-Hernández DA, Almanza-Robles JM. Effect of gallium content and heat treatment on the microstructure and corrosion rate of magnesium binary alloys. Metals (Basel) 2019;9:990. https://doi.org/10.3390/met9090990.
[110] Ishiyama S, Hanada S, Izumi O. Effect of Zr, Sn and Al additions on deformation mode and beta phase stability of metastable beta Ti alloys. ISIJ Int 1991;31:807–13. https://doi.org/10.2355/isijinternational.31.807.
[111] Brozek C, Sun F, Vermaut P, Millet Y, Lenain A, Embury D, et al. A β-titanium alloy with extra high strain-hardening rate: design and mechanical properties. Scripta Mater 2016;114:60–4. https://doi.org/10.1016/j.scriptamat.2015.11.020.
[112] Pourbaix M, Zhang H, Pourbaix A. Atlas of chemical and electrochemical equilibria in the presence of a gaseous phase. 1997. p. 251–4. https://doi.org/10.4028/www.scientific.net/msf.251-254.143.